

Rapid enhancement of radiation belt electron fluxes due to substorm dipolarization of the geomagnetic field

Mei-Ching Fok

Universities Space Research Association, NASA Goddard Space Flight Center, Greenbelt, Maryland

Thomas E. Moore

Laboratory for Extraterrestrial Physics, NASA Goddard Space Flight Center, Greenbelt, Maryland

Walther N. Spjeldvik

Department of Physics, Weber State University, Ogden, Utah

Abstract. The classical pure radial diffusion mechanism appears not to fully explain the frequently observed rapid enhancement in the timescales of minutes to hours in the radiation belt electron fluxes in the Earth's magnetosphere. We here consider other physical mechanisms, such as energization mechanisms associated with substorm processes, to account for these sudden increases. A three-dimensional electron kinetic model is used to simulate the dynamics of the geomagnetically trapped population of radiation belt electrons during a substorm injection event. In the past this model has been extensively used to study dynamics of energetic ions in the ring current. This work, for the first time, constitutes the development of a combined convection and diffusion model to radiation belt electrons in the 0.04–4 MeV kinetic energy range. The Tsyganenko 89 geomagnetic field model is used to simulate the time-varying terrestrial magnetosphere during the growth phase elongation and the expansion phase contraction. We find that inductive electric field associated with the magnetic reconfiguration process is needed in order to transport substorm electrons into the trapped particle region of the magnetosphere. The maximum enhancement in energetic electron fluxes is found to be located around the geosynchronous orbit location ($L = 6.6$), with up to 2 orders of magnitude enhancement in the total fluxes (0.04–4 MeV). Although this enhancement in the inner magnetosphere is very sensitive to the temperature and, to a less extent, density of the source population in the plasma sheet, we suggest that the substorm-associated energization in the magnetotail and the subsequent adiabatic acceleration in the earthward region account for the enhanced MeV electrons (killer electrons) seen at the geosynchronous orbit during storms and substorms.

1. Introduction

Radiation belt electrons are of great interest because they have substantial consequences for processes in the Earth's space environment. They contribute importantly to the penetrating radiation, particularly in deep dielectric charging of surfaces and structures, which may cause significant damage to spacecraft instrumentation and to humans in space. During quiet times, energetic electrons are found in two wide belts around the Earth separated by a "slot" typically located at $L = 2$ –3.5, depending on electron energy. Pitch angle diffusion into the loss cone resulting from interactions with the whistler mode waves in the plasmasphere is believed to be responsible for removing electrons from the slot region [i.e., Lyons *et al.*, 1972]. The inner radiation belt is observed to be very stable, while the outer belt varies significantly with geomagnetic activity. During geomagnetic storm particle injections, radiation belt electrons move earthward into the outer radiation zone and resulting fluxes are enhanced there. The storm-associated radial diffusion then gradually transports particles

inward toward the slot region. The separation between the two electron belts thus becomes shallower or may be completely filled during magnetic storms.

Modeling work has been done to better understand the processes responsible for the radiation belt electron distributions during geomagnetic active times. Bourdarie *et al.* [1996] used the Salammbô code, which solves the diffusion convection equation for the phase space density, to study the stormtime dynamics of the electron radiation belt in an assumed dipolar magnetic field configuration. They also simulated a substorm by injecting keV particles on the nightside at 9 Earth radii (R_E) and found that 100 keV electron were "created" in the ring current region by radial convection of the injected particles.

Particle simulation has been an effective tool to study the dynamics of energetic electrons. Li *et al.* [1993] and Hudson *et al.* [1996] performed guiding center particle simulation of the March 24, 1991, storm sudden commencement (SSC). The former study represented an interplanetary shock using simple electric field model of an asymmetric bipolar pulse and the latter used the electric field output from a global MHI simulation to "push" relativistic electrons. Both studies found a new electron belt was formed on a particle drift timescale due to the SSC-induced electric fields, and this appeared consistent with the CRRES observations.

Copyright 2001 by the American Geophysical Union.

Paper number 2000JA000150.
0148-0227/01/2000JA000150\$09.00

Many studies have been done to investigate the role of substorm inductive electric field in the magnetotail in energization and transport of plasma sheet electrons to the radiation belt region. *Li et al.* [1998] modeled an electron injection event on January 10, 1997, and suggested that dispersionless injection is a consequence of impulsive changes in the electric and magnetic fields originating from the nightside magnetosphere [*Moore et al.*, 1981]. They found that the energization of injected electrons was mainly due to betatron acceleration of the preexisting electron population at larger radial distances in the magnetotail. *Birn et al.* [1998] investigated electron acceleration based on geosynchronous observations and test particle orbits in a MHD simulation of neutral line formation and dipolarization. Their results demonstrated that the dipolarizing field region earthward of the neutral line appeared to be more significant than the neutral line itself for acceleration of electrons. *Kim et al.* [2000] carried out a similar study concentrating primarily on the question of whether substorm processes were sufficient to produce the observed electron enhancement in the outer belt. Their calculations produced only $\sim 2\%$ of the number of MeV electrons seen in a typical MeV-electron event. They noted that, however, the result was very sensitive to the plasma sheet temperature and substorm parameters.

A common conclusion from recent simulations is that classical diffusion mechanism fails to explain the rapid enhancement in a timescale of minutes to hours in the radiation belt electron fluxes. Energization processes associated with substorm processes are asserted to be important to account for these sudden increases. In this paper, the variations of the radiation belt electron distributions inside $10 R_E$ during a substorm injection are simulated using a global three-dimensional model. The study uses a kinetic approach that solves the Boltzmann equation for each plasma species. Particles are assumed to drift in a Tsyganenko magnetic field model [*Tsyganenko*, 1989], which is changed with time to represent the growth phase stretching and expansion phase dipolarization of the magnetic field lines. This kinetic model has previously been used to simulate the enhancement in the ring current proton fluxes and the corresponding poleward expansion of the H^+ precipitation into the ionosphere during dipolarization events [*Fok and Moore*, 1997; *Fok et al.*, 1999]. These simulations generate many frequently observed features of substorm injections, including the sudden appearance of hot plasma tailward of a sharply defined "injection boundary," the earthward motion of an "injection front," the azimuthal and tailward expansion of this enhanced flux region, and the creation of characteristic ion dispersion patterns near geosynchronous orbit. The present model, building on these successful simulations, is for the first time applied to study the radiation belt electrons. Both convective and multimode diffusive processes are considered in a time-varying, nondipolar magnetic field. In the following we proceed to demonstrate that this kinetic electron model is a new and powerful tool that extends our understanding of the mechanisms acting on various timescales that are responsible for the transport and energization of the radiation belt electrons.

2. Kinetic Model of Energetic Plasmas

The temporal variation of the phase space density of a particle species s is calculated by solving the following

bounce-averaged Boltzmann transport equation:

$$\frac{\partial \bar{f}_s}{\partial t} + \langle \dot{\lambda}_i \rangle \frac{\partial \bar{f}_s}{\partial \lambda_i} + \langle \dot{\phi}_i \rangle \frac{\partial \bar{f}_s}{\partial \phi_i} = \frac{1}{\sin 2\lambda_i} \frac{\partial}{\partial \lambda_i} \left(\sin 2\lambda_i D_{\lambda_i \lambda_i} \frac{\partial \bar{f}_s}{\partial \lambda_i} \right) - \frac{\bar{f}_s}{\tau_w} - \left(\frac{\bar{f}_s}{0.5\tau_b} \right)_{\text{loss cone}}, \quad (1)$$

where $\bar{f}_s = \bar{f}_s(t, \lambda_i, \phi_i, M, K)$ is the average distribution function on the field line between mirror points. Variables λ_i and ϕ_i are the magnetic latitude and local time, respectively, at the ionosphere foot point of the geomagnetic field line. M is the relativistic magnetic moment and $K = J/\sqrt{8m_0M}$, where J is the second adiabatic invariant. The motion of the particles is described by their drifts across field lines which are labeled by their ionospheric foot points. The shape of a field line changes, but the ionospheric foot points are treated to be fixed [*Birmingham and Jones*, 1968] and essentially dipolar. In this study, the ranges of the four variables in the spatial-velocity space are λ_i , 43° – 68° ; ϕ_i , 0 – 24 hours; M , 0.07 – 4.3×10^4 MeV/G; K , 60 – 1.5×10^5 T $^{0.5}$ m.

The calculation of the bounce-averaged drift velocities $\langle \dot{\lambda}_i \rangle$ and $\langle \dot{\phi}_i \rangle$ were described in detail in the paper of *Fok and Moore* [1997]. And therefore only a brief description is given here. Velocities $\langle \dot{\lambda}_i \rangle$ and $\langle \dot{\phi}_i \rangle$ can be expressed as

$$\langle \dot{\lambda}_i \rangle = -\frac{1}{q\xi} \frac{\partial H}{\partial \phi_i} \quad (2)$$

$$\langle \dot{\phi}_i \rangle = \frac{1}{q\xi} \frac{\partial H}{\partial \lambda_i},$$

where $\xi = M_E \sin 2\lambda_i / r_i$, M_E is the Earth's magnetic dipole moment, and r_i is the radial distance of the ionospheric foot point of a field line. In this study, we assume $r_i = 1.126 R_E$, which corresponds to ~ 800 km in altitude. H is the Hamiltonian and has the expression

$$H = \sqrt{p^2 c^2 + m_0^2 c^4} + q\Phi - q\Omega \frac{M_E}{2r_i} \cos 2\lambda_i, \quad (3)$$

in which Φ is the cross-tail convection potential and Ω is the angular velocity of the rotation of the Earth itself. The derivatives of the first, second, and third terms on the right-hand side of (3) correspond to the geomagnetic gradient-curvature drift, electric drift (convection) and corotation, respectively, of a charged particle. Based on the assumption of "frozen in field line," the induced electric field due to changing magnetic configuration is treated implicitly by mapping the particle trajectory and distribution from the ionosphere to the equator along field lines that are modeled to vary with time. In the numerical computation the value of H and thus the drift velocities, are continuously updated according to the instantaneous configuration of the magnetosphere [*Fok and Moore*, 1997].

The first term on the right-hand side of (1) represents particle diffusion in λ_i as a result of electric and magnetic fluctuations. Diffusion in latitude in the ionosphere is equivalent to radial diffusion in the magnetosphere (i.e., at the equator). Equation (1) thus represents a combined convection-diffusion approach in solving for the electron radiation belt distribution. During magnetic storms and substorms, the magnetic and electric fields undergo large-scale variations or reconfigurations. This global topology structure and its

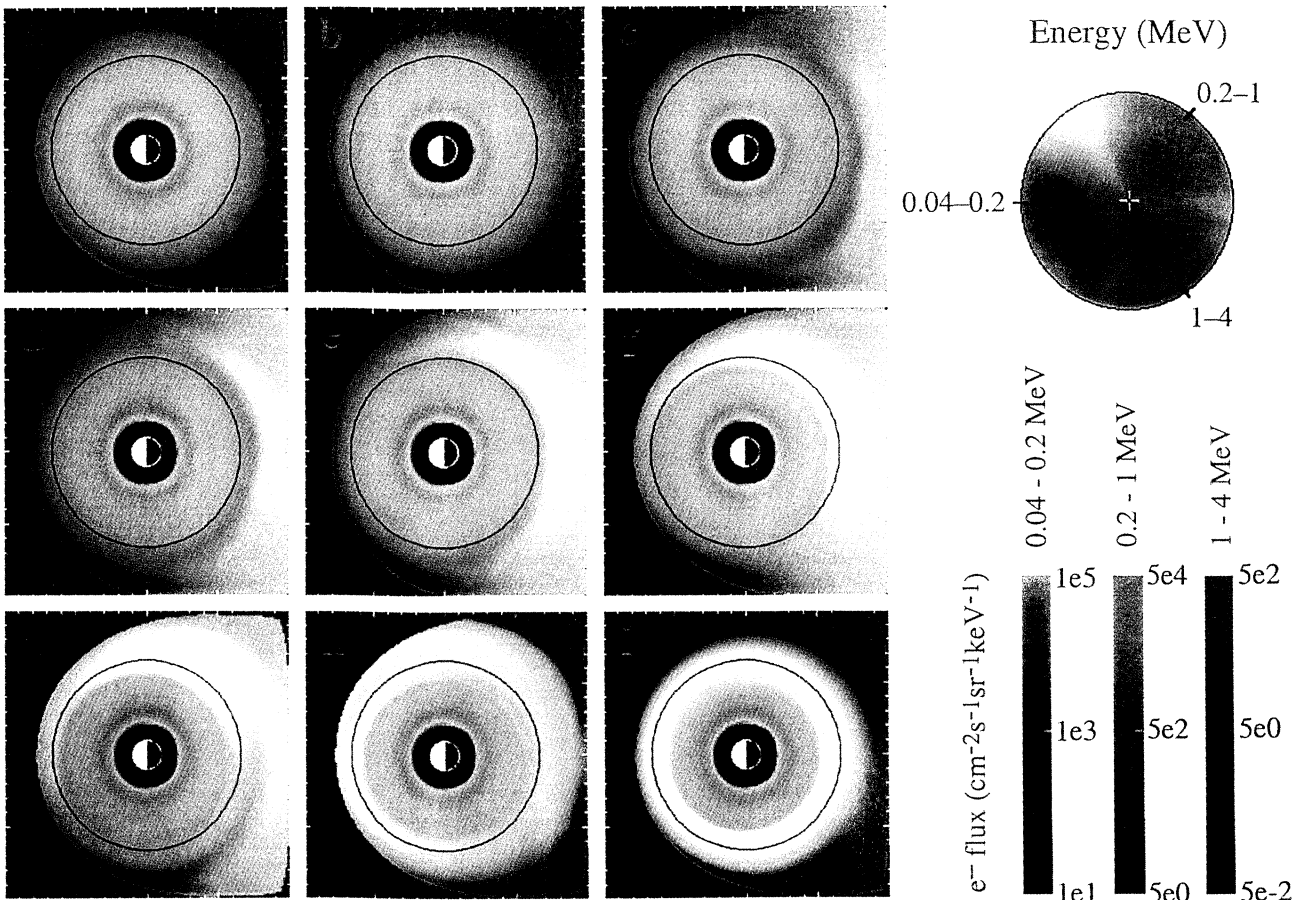
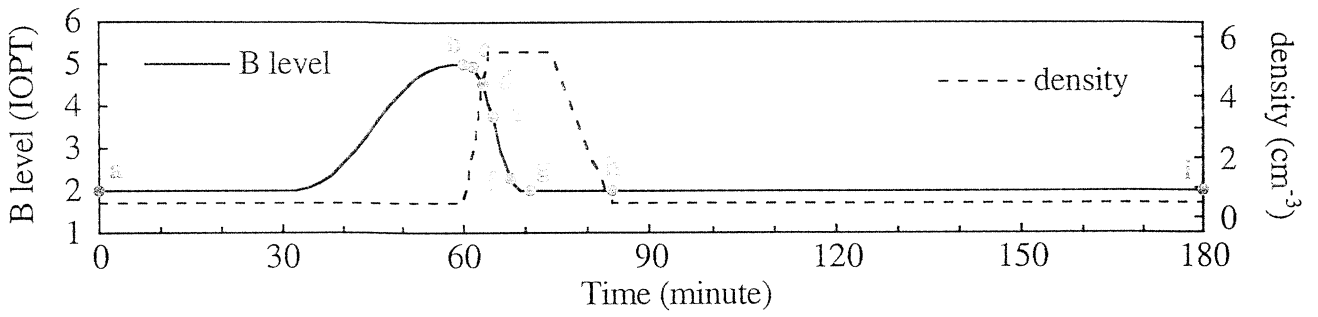


Plate 1. Simulated temporal evolution of electron fluxes at the equator. Electrons with energies 0.04–0.4, 0.4–1 and 1–4 MeV are represented by red, green and blue colors, respectively. The contents in Plates 1a–1i correspond to the time label in the top panel. Black circles are the geosynchronous orbits.

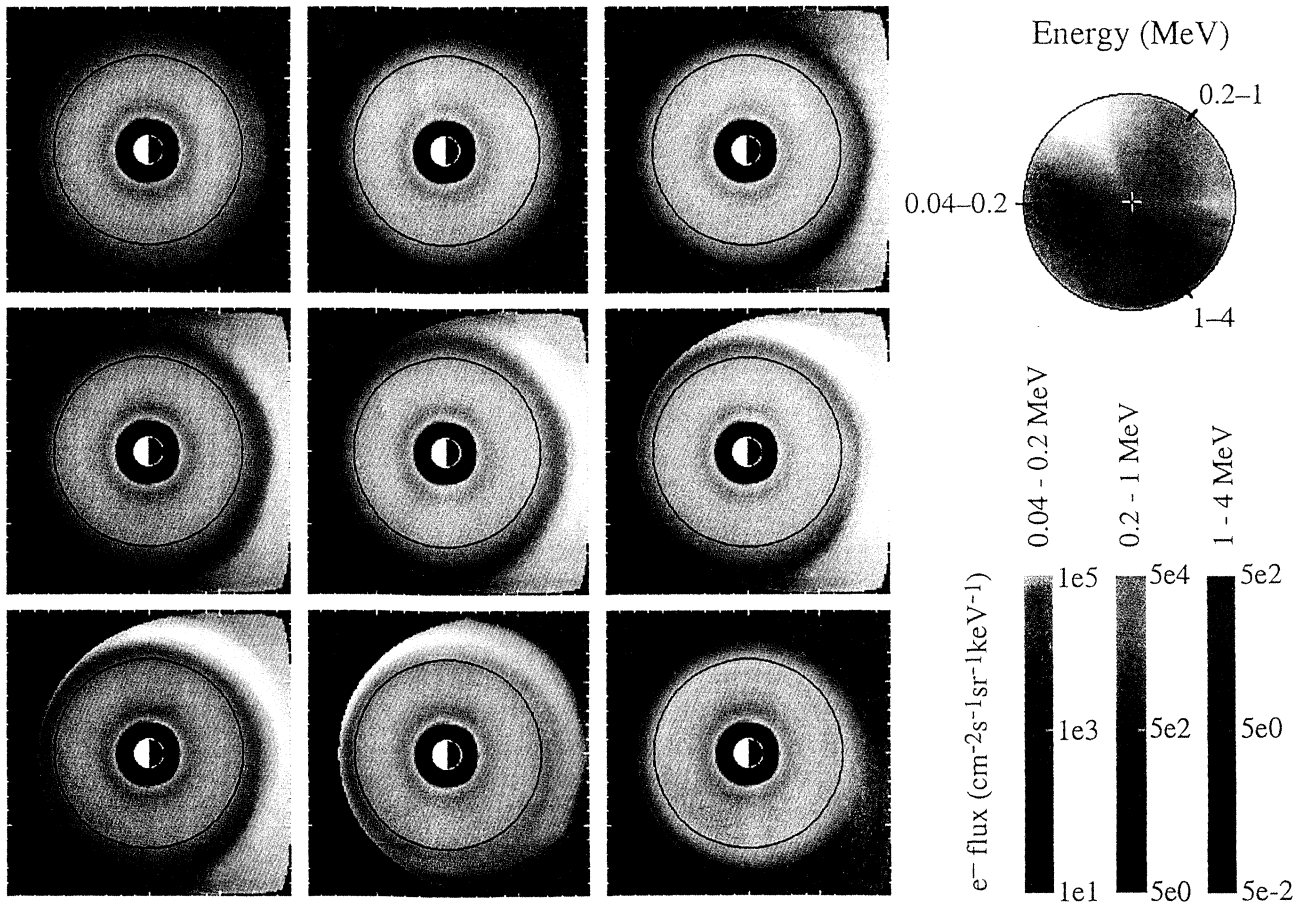
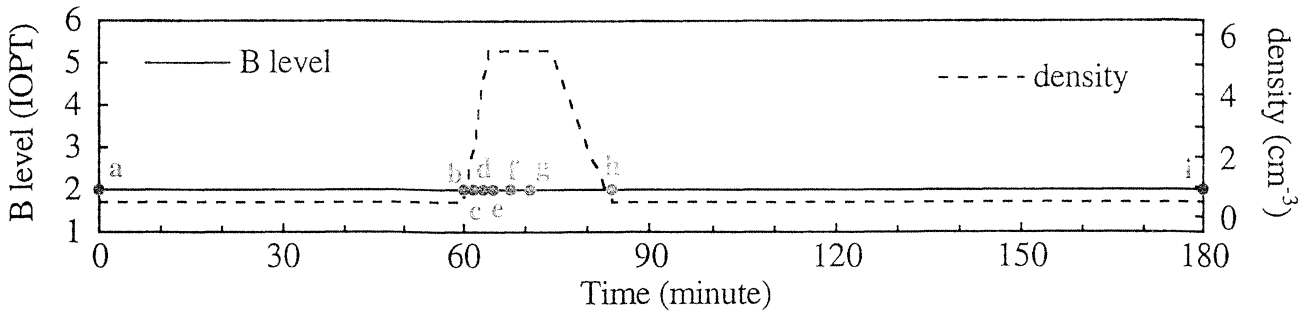


Plate 2. Same as Plate 1 except the magnetic field configuration is kept constant during the simulation.

dynamic changes determines the overall charged particle convection transport patterns. At the same time, **B** and **E** continually fluctuate over a range of oscillation frequencies and amplitudes. With a specific form of the power spectrum adopted, an appropriate radiation belt diffusion coefficients can be formulated either expressed as functions of the *L* shell parameter or, equivalently, as functions of the invariant magnetic latitude as indicated in (1). By considering both convection and diffusion simultaneously, we can realistically simulate the convection-dominated low-energy particles, the diffusion-dominated high-energy particles, and the ring current range where both processes are effective. Furthermore, we are able to resolve the transient behaviors of plasmas due to the rapid magnetic-electric reconfiguration from the comparatively long timescale diffusion effects. The derivation of the diffusion term in (1) is given in the Appendix A. The diffusion term is followed by a description of the loss terms of electrons. Variable τ_w is the precipitation lifetime resulting from electron pitch angle diffusion into the loss cone due to interactions with plasmaspheric whistler mode waves. These electron lifetimes have been given by Lyons *et al.* [1972] and are used in this work. Particles in the loss cone, the boundary of which is assumed to correspond to mirror height of 800 km, are assumed to have a lifetime of one half bounce period ($0.5\tau_b$).

3. Models Used, Initial and Boundary Conditions

In order to simulate the particle dynamics in a changing magnetospheric configuration, the empirical model of Tsyganenko 89 (EXT89KP [Tsyganenko, 1989]) has been used to model the time-varying magnetosphere during the growth phase elongation and the expansion phase contraction of the substorm process. The top panel in Figure 1 shows the assumed magnetic field configuration level (IOPT) as a function of time. Low configuration level was constructed by magnetic data taken when *Kp* is low and thus represents a quiet dipole-like magnetosphere, and high configuration level represents an active, stretched magnetotail. As shown in Figure 1, the evolution of the energetic electron population in a 3-hour substorm event period is simulated. The magnetosphere is at configuration 2 in the first 30 min and then grows from configuration 2 to 5 in the next 30 min. Right after reaching configuration level 5 the magnetosphere returns to configuration level 2 in 10 min and stays at this configuration during the rest of the simulation. The rise and the decline of the magnetic field configuration shown in Figure 1 are fitted by polynomials of degree 5 to ensure zero values of the inductive electric field and its time derivative at the beginning and the end of transition [Delcourt *et al.*, 1990]. The convection electric field is assumed to be Volland-Stern type

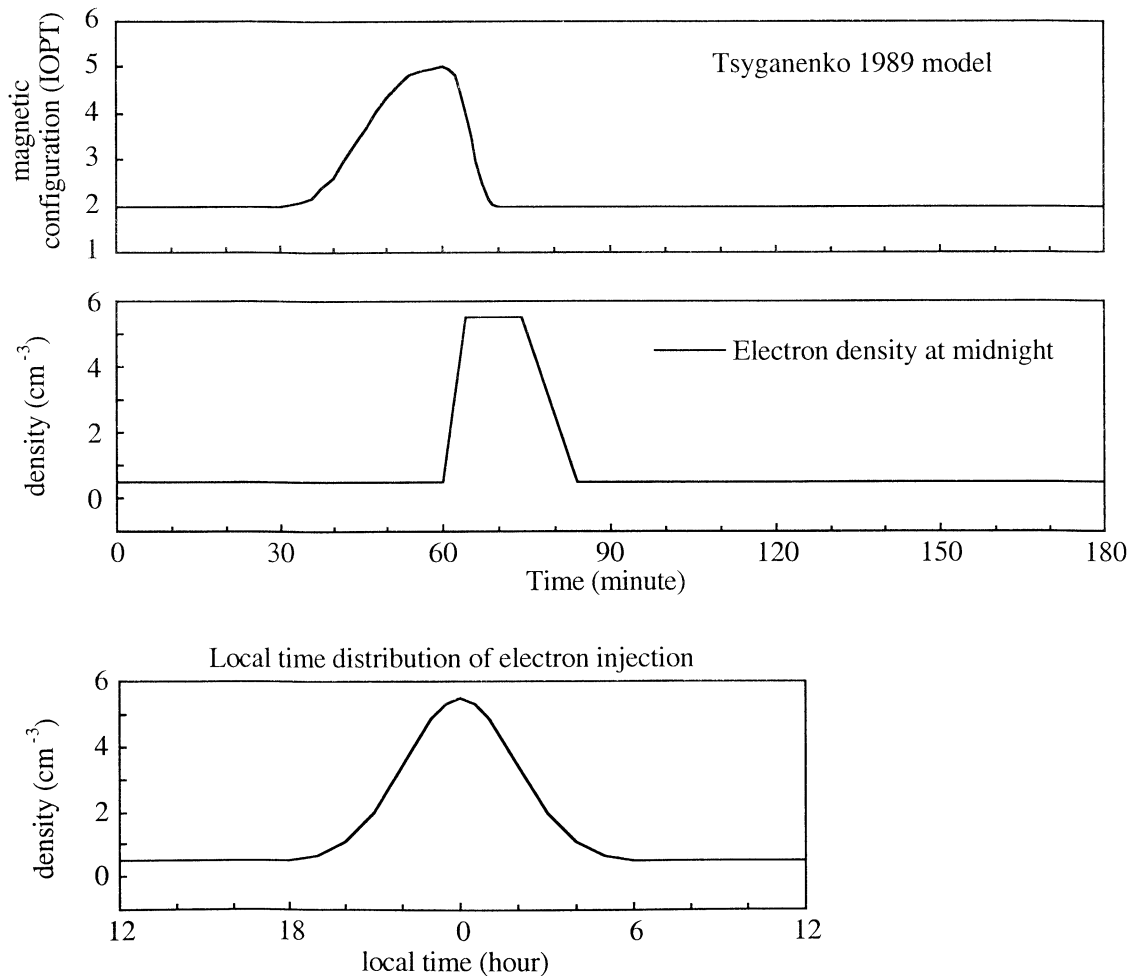


Figure 1. (top) Simulated magnetospheric configuration as a function of time. The field configurations are according to the Tsyganenko 1989 magnetic field model. (middle) Modeled density of injected energetic electrons at 10 R_E . (bottom) Longitudinal dependence of injected electron density.

[Volland, 1973; Stern, 1975], with convection reversal boundary set at 72° latitude and cross-polar cap potential drop of 100 kV. The convection electric field is here kept constant with time.

In the ionosphere the magnetic field is approximated by a dipole and $r_i = L \cos^2 \lambda_i$. The diffusion coefficient in (1), $D_{\lambda_i \lambda_i}$, is thus related to D_{LL} as

$$D_{\lambda_i \lambda_i} = D_{LL} \left(\frac{\partial \lambda_i}{\partial L} \right)^2 = D_{LL} \frac{\cos^4 \lambda_i}{r_i \sin 2\lambda_i}, \quad (4)$$

where r_i is the radial distance in R_E of the ionospheric reference location. D_{LL} applied here has the form [Cornwall, 1972; Spjeldvik, 1996]

$$D_{LL} = C_m L^{10} + \frac{C_e L^{10}}{L^4 + (M/\gamma)^2}, \quad (5)$$

where M is magnetic moment in MeV/G and γ is the ratio of total energy to rest mass energy. In this study we assume a moderate radial diffusion with $C_m = 2 \times 10^{-14} \text{ s}^{-1}$ and $C_e = 8 \times 10^{-11} \text{ s}^{-1}$.

Mathematically, (1) represents an initial boundary value problem. In this study, the initial conditions are specified by the NASA trapped radiation model AE 8 (SOLMAX) [e.g., Fung, 1996], and they are assumed to be both local time symmetric and isotropic in pitch angle. The boundary flux at $10 R_E$ equatorial distance at all local times is assumed to be a kappa distribution

$$j(\mathbf{r}, E) = n(\mathbf{r}) \frac{\Gamma(\kappa + 1)}{(\pi\kappa)^{3/2} \Gamma(\kappa - 1/2)} \left(\frac{E^2}{2m_0 E_0^3} \right)^{1/2} \left(1 + \frac{E}{\kappa E_0} \right)^{-\kappa - 1} \quad (6)$$

with $\kappa = 4$, assuming a density (n) of 0.5 cm^{-3} and a characteristic energy (E_0) 1 keV, consistent with the AE 8 model. However, during the expansion phase of the substorm, an additional electron population is superposed upon the baseline distribution to represent the enhanced plasma sheet. This feature is always observed during disturbed geomagnetic conditions [Christon *et al.*, 1991; Borovsky *et al.*, 1997]. We assume that the injected electron population is also a kappa distribution with $\kappa = 4$, but with the higher density of 5 cm^{-3} and an elevated characteristic energy of 5 keV. The injected electrons in the midnight sector at the $10 R_E$ boundary are assumed to rise to the peak intensity at 64 min, 4 min after the substorm onset, and are further assumed to stay at high intensity for 10 minutes and then are taken to linearly decay toward zero during the next 10 min (middle panel, Figure 1). The longitudinal (local time) dependence of the injected electrons is shown in the bottom panel of Figure 1. It is fitted by a Gaussian distribution with a variance (2 hour)², peaking at tail center.

4. Electron Enhancement During Substorm Injection

The kinetic equation (1) is solved with the initial distribution, boundary condition, diffusion, precipitation loss, electric and magnetic configurations specified in the previous sections. The electron differential flux j_s is then calculated by $j_s = p^2 f_s$. The temporal evolution of the pitch angle averaged fluxes at the equator is shown in Plate 1, in which particles with energies 0.04–0.2, 0.2–1, and 1–4 MeV

are represented by red, green, and blue, respectively. The three color bars show the intensity scales for each energy range. Note that the three scales are different such that all three colors can be seen. In Plate 1, for example, intensity (in $\text{cm}^{-2} \text{ s}^{-1} \text{ sr}^{-1} \text{ keV}^{-1}$) of 1×10^3 in the 0.04–0.2 MeV energy range will have the same brightness as intensity of 5×10^2 in the 0.2–1 MeV range. In this representation, yellow color signifies the existence of low- and medium-energy electrons but lack of high-energy particles. Similarly, magenta color represents a mix of low- and high-energy plasmas with deficiency of particles at medium energies.

Plate 1 shows that the magnetosphere is expanding during the time interval from 30 to 60 min (Plate 1b). We find that the electron distribution does not change noticeably during this period of growth phase. Then the electron density at the nightside boundary starts to rise (Plate 1c). These freshly injected plasmas convect earthward in response to the cross-tail electric field, and in response to the inductive electric field as the geomagnetic field lines are dipolarizing. As particles reach the radial distance where magnetic azimuthal drifts are strong, they drift azimuthally around the Earth and become parts of the geomagnetically trapped population (Plates 1d to 1g).

When the electrons drift from the nightside to the dayside where the magnetic field is more compressed, they are also adiabatically energized and particles with higher energies drift faster around the Earth. Plate 1f clearly shows the separation of electrons with different kinetic energies: yellow color (~0.2 MeV) in the postmidnight sector, green color (~0.5 MeV) in the prenoon sector and magenta color (0.1 and 2 MeV without 0.5 MeV) in the postnoon sector. Near the end of the particle injection (Plate 1h), all of the injected electrons in the 0.04–4 MeV energy range have reached the dusk and the premidnight sector. As a result, the local time asymmetry in energy distribution is then largely reduced. The injected electrons form a new radiation belt around the Earth near the geosynchronous orbit distance (Plate 1i) and will remain in that region of space with quite high intensity for many hours and/or several days according to their decay lifetimes.

We have shown that the convection and inductive electric fields transport plasma sheet electrons inward to the geomagnetic confinement and trapping region and thus create a newly injected electron radiation belt. In order to separate the effects of inductive field from the convection field, we have done a test run in which the Tsyganenko magnetic field is kept at configuration 2 throughout the 3-hour simulation. The convection electric field, the strength of particle injection and all other conditions, are the same as the original run. Plate 2 shows the results of this test simulation. The flux enhancements start at time c . The injected electrons then drift eastward to the dayside. However, most injected particles are lost in the vicinity of the dayside boundary before they can reach the duskside. At the end of particle injection, only a minor flux enhancement is found. Plate 2 amply illustrates that, in addition to strong convection, other energization and transport processes, such as substorm expansion, are necessary to allow deep penetration of substorm associated plasmas and to produce a robust trapped radiation belt population.

We have also performed another test run in which the geomagnetic field undergoes expansion and compression as shown in Figure 1. Nevertheless the electron flux distributions at the $10 R_E$ boundary remain at their initial

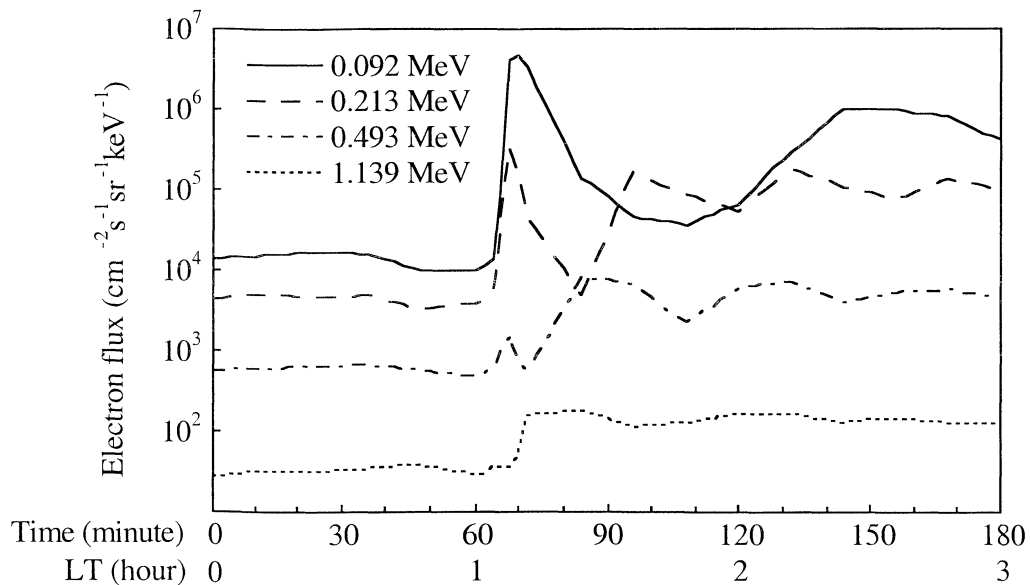


Figure 2. Electron fluxes of four energies seen by a virtual geosynchronous spacecraft during the injection event.

values and do not change with time. We found that (results not shown) during the substorm expansion phase, the outer belt is energized and transported earthward by the inductive electric field. However, we also found that there is only a 24% increase in the total energy content of the electron population within $10 R_E$ during the dipolarization. In contrast, the corresponding increase in particle energy in the original run (Plate 1) is 160%. This test run has clearly shown the importance of plasma sheet preconditioning [e.g., *Kozyra et al.*, 1998] in magnetic storm and substorm growth. The storm and substorm development can be divided into two steps. First the plasma sheet is enhanced in both temperature and particle density as results of the energization processes in the magnetotail [Delcourt and Sauvaud, 1994; Fok et al., 1999]. Then the enhanced plasma sheet particles are further energized and carried into the inner magnetosphere by the convection and inductive electric fields.

Substorm injections are frequently seen by geosynchronous satellites. Fast injection signatures at the geostationary orbit are often used to identify the timings of substorm development. In Plate 1 we have shown that the maximum electron flux enhancement occurs around the geosynchronous orbit. Next we fly a virtual geosynchronous satellite during this substorm and evaluate whether our model can reproduce the electron injection features that have been observed in the magnetosphere in such situations [e.g., *Reeves et al.*, 1998]. Figure 2 plots the computed electron fluxes at various energies that would be seen by the virtual spacecraft. The virtual satellite rotates with the Earth and is at midnight at time = 0. Strong injection of 92 and 213 keV electrons are seen right after the onset of the injection event at 60 min. For the higher energies (493 keV and 1.139 MeV) with large drift velocities, these electrons rapidly drift eastward from midnight and pass the observation point at 0100 LT. As a result of this, only a small enhancement of 493 keV electrons is actually seen at ~ 65 min. For the 1.139 MeV electrons they drift even faster and are seen by the satellite only after they have completed cycling around the Earth once. The signature of drift echo is

also reproduced in the simulation. It is found that the echo periods are consistent with the particle drift periods, as one would expect. The echo feature is fairly obvious in the virtual data at low electron energies but this feature becomes more convoluted (smeared) for fast-drifting plasmas (i. e., for 1.139 MeV electrons in our case).

As shown in Figure 2, our simulation predicts a factor of 5 increase in the MeV electrons at the geosynchronous orbit, the so-called "killer electrons." The MeV electron flux reaches a level of $10^2 \text{ cm}^{-2} \text{ s}^{-1} \text{ sr}^{-1} \text{ keV}^{-1}$, which is typical for a strong electron event. Our simulated electron enhancement at the geosynchronous is very sensitive to the temperature of the injected plasma sheet electrons at $10 R_E$, consistent with what *Kim et al.* [2000] have found. In the cases of strong repeated dipolarizations, the energization in the magnetotail would produce higher temperature than we have assumed in this study (5 keV). Therefore it is clear that substorm energization in the plasma sheet and the subsequent adiabatic acceleration in the inner region are sufficient to produce the killer electrons observed during substorms and particularly series of substorms associated with storms.

5. Discussion and Conclusion

We have extended our earlier studies of magnetic storms and substorms to derive a convection-diffusion model of radiation belt electrons. The model is based on our ring current model which has been used previously to simulate the ring current development and to study the relationship between substorm and storms [Fok et al., 1996, 1999]. The model herein reported has the capability to adapt to more realistic, time varying magnetic and electric field configurations. As the model is extended to higher energies, both convection and induction are still important to resolve local time and energy dependent features during substorms, as we have shown here. Moreover, radial diffusion is clearly the dominant longer term process populating the outer radiation belt and the slot region during the recovery phase of storms. Furthermore, substorm

effects can be treated as diffusive over sufficiently long timescales when prediction of local or peak conditions is not paramount.

Energetic particle decay owing to various losses along particle drift trajectories can be easily calculated within the framework of this combined convection-diffusion model. For energetic electrons, interactions with various wave modes are crucial in producing the slot region either as a long-term quasi-steady feature or as a dynamically evolving structure [Lyons *et al.*, 1972]. Plasma waves can also be important in accelerating the relativistic electrons in the magnetosphere [Elkington *et al.*, 1999]. These wave particle interactions can be implemented in our transport model as descriptions of the corresponding diffusion coefficients. However, when we simulate short timescale injections, radial diffusion and wave losses are relatively unimportant, and their importance come into play primarily on longer residence timescales in the inner magnetosphere.

In the modeling presented in this paper we have constructed a time-dependent boundary condition at $10 R_E$ without resorting to the extensive particle trajectory backtracking used in our earlier study [Fok *et al.*, 1999]. However, we used that study as a practical guide to the boundary time dependence, matching our assumed electron density with our computed ion density in the earlier study. Thus the focus herein is on the effects of dipolarization on the energetic electron populations of the outer radiation belt, rather than on the preconditioning of the plasma sheet.

In conclusion, we have developed a global 3-D convection and diffusion model to realistically simulate the transport and energization of the radiation belt plasmas. This model is a powerful tool that extends capabilities previously brought to bear on this problem. With further implementation and development, this model can be used to predict and forecast the radiation belt environment. In the simulation of an electron injection event during a magnetic dipolarization, we find the following characteristic features.

1. The major source of electrons leading to flux enhancements during substorms is freshly injected particles from the central plasma sheet region. The level of enhancement is very sensitive to the temperature and, to less extent, density of the plasma sheet.

2. A traveling electron "injection front" is formed, which advances earthward and eastward starting near midnight.

3. At the end of the injection phase, an inner electron injection boundary is formed that is roughly circular and lies somewhat inside of the geosynchronous orbit.

4. Following the injection phase, the energetic electrons disperse in local time in a way that is consistent with the well-known patterns associated with the injection boundary formation. In particular, clear and characteristic electron drift echoes are produced at the higher energies.

5. The effect of the dipolarization-associated induction electric field is to transfer the energetic electrons into the trapped region and to produce a new radiation belt near the geosynchronous orbit. However, with strong convection alone, most energetic electrons injected into the nightside sector will drift around the Earth and be lost at the dayside magnetopause.

6. The substorm associated energization in the magnetotail and the subsequent adiabatic acceleration in the earthward region are sufficient to produce the enhanced MeV electrons

seen at the geosynchronous orbit during substorms and series of substorms associated with storms.

Appendix A: Diffusion Equation of λ_i

We start the derivation of the diffusion term in (1) by the gyroaveraged diffusion equation of λ_i

$$\frac{\partial f_s}{\partial t} = \frac{1}{G} \frac{\partial}{\partial \lambda_i} \left(GD_{\lambda_i} \frac{\partial f_s}{\partial \lambda_i} \right), \quad (\text{A1})$$

where $f_s = f_s(s, \phi_i, M, K, \lambda_i)$. G is the pertinent Jacobian defined as

$$\frac{1}{G} = \frac{dsd\phi_i dM dK d\lambda_i}{d^3 r d^3 p}, \quad (\text{A2})$$

in which

$$d^3 r = dA_{\perp} ds = \frac{B_r}{B} (dA_{\perp})_i ds, \quad (\text{A3})$$

where dA_{\perp} is the cross section of the differential flux tube perpendicular to \mathbf{B} . Subscript i represents values at the ionosphere location. Equation (A3) can be further expanded using

$$(dA_{\perp})_i = (dA \hat{b} \cdot \hat{r})_i = r_i^2 \cos \lambda_i d\lambda_i d\phi_i \left(\frac{B_r}{B} \right)_i. \quad (\text{A4})$$

Substituting (A4) into (A3), we have

$$d^3 r = \frac{r_i^2 \cos \lambda_i (B_r)_i}{B} d\lambda_i d\phi_i ds. \quad (\text{A5})$$

On the other hand, $d^3 p = 2(2\pi p_{\perp} dp_{\parallel} dp_{\perp})$. Therefore (A2) becomes

$$\frac{1}{G} = \frac{B}{4\pi p_{\perp} r_i^2 \cos \lambda_i (B_r)_i} \left| \begin{array}{cc} \left(\frac{\partial M}{\partial p_{\parallel}} \right)_{p_{\perp}} & \left(\frac{\partial K}{\partial p_{\parallel}} \right)_{p_{\perp}} \\ \left(\frac{\partial M}{\partial p_{\perp}} \right)_{p_{\parallel}} & \left(\frac{\partial K}{\partial p_{\perp}} \right)_{p_{\parallel}} \end{array} \right|. \quad (\text{A6})$$

It can be shown that

$$\left(\frac{\partial M}{\partial p_{\parallel}} \right)_{p_{\perp}} = 0 \quad (\text{A7})$$

$$\left(\frac{\partial M}{\partial p_{\perp}} \right)_{p_{\parallel}} = \frac{p_{\perp}}{m_o B} \quad (\text{A8})$$

$$\left(\frac{\partial K}{\partial p_{\parallel}} \right)_{p_{\perp}} = \mu T(y) \sqrt{\frac{1}{2m_o M}}, \quad (\text{A9})$$

where μ is the pitch cosine, y is sine of the equatorial pitch angle, and $T(y) = \int_{s_m}^{s_m} ds / \mu$. Putting (A7) through (A9) into (A6), we have

$$G = \frac{4\pi r_i^2 \cos \lambda_i (B_r)_i}{\mu T(y)} \sqrt{2m_o^3 M}. \quad (\text{A10})$$

Substituting (A10) into (A1) and carrying out bounce average of (A1), we obtain

$$\begin{aligned} \frac{\partial \bar{f}_s}{\partial t} &= \frac{1}{\cos \lambda_i (B_r)_i} \frac{\partial}{\partial \lambda_i} \left(\cos \lambda_i (B_r)_i \left\langle D_{\lambda_i, \lambda_i} \right\rangle \frac{\partial \bar{f}_s}{\partial \lambda_i} \right) \\ &= \frac{1}{\sin 2\lambda_i} \frac{\partial}{\partial \lambda_i} \left(\sin 2\lambda_i \left\langle D_{\lambda_i, \lambda_i} \right\rangle \frac{\partial \bar{f}_s}{\partial \lambda_i} \right), \end{aligned} \quad (\text{A11})$$

where $\langle D_{\lambda_i, \lambda_i} \rangle$ is the bounce-averaged D_{λ_i, λ_i} . Since the characteristic time for diffusion is usually much longer than the bounce period (excluding the limiting condition of strong diffusion), $\langle D_{\lambda_i, \lambda_i} \rangle$ can be replaced by D_{λ_i, λ_i} and (A11) could be rewritten as

$$\frac{\partial \bar{f}_s}{\partial t} = \frac{1}{\sin 2\lambda_i} \frac{\partial}{\partial \lambda_i} \left(\sin 2\lambda_i D_{\lambda_i, \lambda_i} \frac{\partial \bar{f}_s}{\partial \lambda_i} \right). \quad (\text{A12})$$

Acknowledgments. We thank Richard Wolf, Tsugunobu Nagai, George Khazanov, and Xinlin Li for useful discussions. This work was supported by the NASA Office of Space Science under UPN432-20-00 and 344-14-10 and by grant NAG5-4968 to the Universities Space Research Association.

Janet G. Luhmann thanks referees for their assistance in evaluating this paper.

References

- Birmingham, T. J., and F. C. Jones, Identification of moving magnetic field lines, *J. Geophys. Res.*, **73**, 5505-5510, 1968.
- Birn, J., M. F. Thomsen, J. E. Borovsky, G. D. Reeves, D. J. McComas, R. D. Belian, and M. Hesse, Substorm electron injections: Geosynchronous observations and test particle simulations, *J. Geophys. Res.*, **103**, 9235-9248, 1998.
- Borovsky, J. E., M. F. Thomsen, and D. J. McComas, The superdense plasma sheet: Plasmaspheric origin, solar wind origin, or ionospheric origin? *J. Geophys. Res.*, **102**, 22,089-22,097, 1997.
- Bourdarie, S., D. Boscher, and T. Beutier, Dynamic physical modeling of trapped particles for satellite survey, in *Radiation Belts: Models and Standards*, *Geophys. Monogr. Ser.*, vol. 97, edited by J. F. Lemaire, D. Heynderickx, and D. N. Baker, pp. 27-33, AGU, Washington, D. C., 1996.
- Christon, S. P., D. J. Williams, D. G. Mitchell, C. Y. Huang, and L. A. Frank, Spectral characteristics of plasma sheet in and electron populations during disturbed geomagnetic conditions, *J. Geophys. Res.*, **96**, 1-22, 1991.
- Cornwall, J. M., Radial diffusion of ionized helium and protons: A probe for magnetospheric dynamics, *J. Geophys. Res.*, **77**, 1756-1770, 1972.
- Delcourt, D. C., and J. A. Sauvaud, Plasma sheet ion energization during dipolarization events, *J. Geophys. Res.*, **99**, 97-108, 1994.
- Delcourt, D. C., J. A. Sauvaud, and A. Pedersen, Dynamics of single particle orbits during substorm expansion phase, *J. Geophys. Res.*, **95**, 20,853-20,865, 1990.
- Elkington, S. R., M. K. Hudson, and A. A. Chan, Acceleration of relativistic electrons via drift-resonant interaction with toroidal-mode Pc-5 ULF oscillations, *Geophys. Res. Lett.*, **26**, 3273-3276, 1999.
- Fok, M.-C., and T. E. Moore, Ring current modeling in a realistic magnetic field configuration, *Geophys. Res. Lett.*, **24**, 1775-1778, 1997.
- Fok, M.-C., T. E. Moore, and M. E. Greenspan, Ring current development during storm main phase, *J. Geophys. Res.*, **101**, 15,311-15,322, 1996.
- Fok, M.-C., T. E. Moore, and D. C. Delcourt, Modeling of inner plasma sheet and ring current during substorms, *J. Geophys. Res.*, **104**, 14,557-14,569, 1999.
- Fung, S. F., Recent development in the NASA trapped radiation model, in *Radiation Belts: Models and Standards*, *Geophys. Monogr. Ser.*, vol. 97, edited by J. F. Lemaire, D. Heynderickx, and D. N. Baker, pp. 79-91, AGU, Washington, D. C., 1996.
- Hudson, M. K., S. R. Elkington, J. G. Lyon, V. A. Marchenko, I. Roth, M. Temerin, and M. S. Gussenhoven, MHD/particle simulations of radiation belt formation during a storm sudden commencement, in *Radiation Belts: Models and Standards*, *Geophys. Monogr. Ser.*, vol. 97, edited by J. F. Lemaire, D. Heynderickx, and D. N. Baker, pp. 57-62, AGU, Washington, D. C., 1996.
- Kim, H.-J., A. A. Chan, R. A. Wolf, and J. Birn, Can substorms produce relativistic outer belt electrons? *J. Geophys. Res.*, **105**, 7721-7735, 2000.
- Kozyra, J. U., J. E. Borovsky, M. W. Chen, M.-C. Fok, and V. K. Jordanova, Plasma sheet preconditioning, enhanced convection, and ring current development, in *Substorms-4*, edited by S. Kokubun and Y. Kamide, pp. 755-760, Terra Sci. Publishing Co., Tokyo, 1998.
- Li, X., I. Roth, M. Temerin, J. Wygant, M. K. Hudson, and J. B. Blake, Simulation of the prompt energization and transport of radiation belt particles during the March 23, 1991, SSC, *Geophys. Res. Lett.*, **20**, 2423-2426, 1993.
- Li, X., D. N. Baker, M. Temerin, G. D. Reeves, and R. D. Belian, Simulation of dispersionless injections and drift echoes of energetic electrons associated with substorms, *Geophys. Res. Lett.*, **25**, 3763-3766, 1998.
- Lyons, L. R., R. M. Thorne, and C. F. Kennel, Pitch-angle diffusion of radiation belt electrons with the plasmasphere, *J. Geophys. Res.*, **77**, 3455-3474, 1972.
- Moore, T. E., R. L. Arnoldy, J. Feynman, and D. A. Hardy, Propagating substorm injection fronts, *J. Geophys. Res.*, **86**, 6713-6726, 1981.
- Reeves, G. D., R. H. W. Friedel, R. D. Belian, M. M. Meier, M. G. Henderson, T. Onsager, H. J. Singer, D. N. Baker, X. Li, and J. B. Blake, The relativistic electron response at geosynchronous orbit during the January 1997 magnetic storm, *J. Geophys. Res.*, **103**, 17,559-17,570, 1998.
- Spjeldvik, W. N., Cross field entry of high charge state energetic heavy ions into the Earth's magnetosphere, in *Radiation Belts: Models and Standards*, *Geophys. Monogr. Ser.*, vol. 97, edited by J. F. Lemaire, D. Heynderickx, and D. N. Baker, pp. 63-67, AGU, Washington, D. C., 1996.
- Stern, D. P., The motion of a proton in the equatorial magnetosphere, *J. Geophys. Res.*, **80**, 595-599, 1975.
- Tsyganenko, N. A., A magnetospheric magnetic field model with a warped tail current sheet, *Planet. Space Sci.*, **37**, 5-20, 1989.
- Volland, H., A semiempirical model of large-scale magnetospheric electric fields, *J. Geophys. Res.*, **78**, 171-180, 1973.
- M.-C. Fok, NASA Goddard Space Flight Center, Code 692, Greenbelt, MD 20771. (mei-ching.fok@gsfc.nasa.gov)
- T. E. Moore, NASA Goddard Space Flight Center, Code 692, Greenbelt, MD 20771.
- W. N. Spjeldvik, Department of Physics, Weber State University, Ogden, UT 84408.

(Received April 19, 2000; revised September 14, 2000; accepted September 14, 2000.)